Electrochimica Acta 222 (2016) 1792–1799

Contents lists available at ScienceDirect

Electrochimica Acta

journal homepage: www.elsevier.com/locate/electacta

Method for studying high temperature aqueous electrochemical systems: Methanol and glycerol oxidation

Thomas Holm[a,b], Per Kristian Dahlstrøm[a,b], Odne S. Burheim[c], Svein Sunde[a], David A. Harrington[b], Frode Seland[a,*]

[a] Department of Materials Science and Engineering, Norwegian University of Science and Technology, NO-7491 Trondheim, Norway
[b] Department of Chemistry, University of Victoria, Victoria, British Columbia, V8W 3V6, Canada
[c] Department of Electrical Engineering and Renewable Energy, Norwegian University of Science and Technology, NO-7491 Trondheim, Norway

ARTICLE INFO

Article history:
Received 8 September 2016
Received in revised form
22 November 2016
Accepted 22 November 2016
Available online 29 November 2016

Keywords:
Pt electrodes
Electrocatalysis
Methanol
Glycerol
Temperature

ABSTRACT

A method for high purity aqueous electrochemical experiments at temperatures above the normal boiling point of water and at temperatures up to 140 °C is described. A three-electrode cell in a self-pressurized glass autoclave is heated in an oil bath. Slow ramping of the temperature allows efficient acquisition of kinetic parameters such as activation energies, oxidation onset potentials and Tafel slopes by using cyclic voltammetry. The oxidation of two organic alcohols with different volatilities, methanol (high volatility) and glycerol (low volatility), are studied to demonstrate the capabilities of the method. Methanol oxidation on platinum is found to have a similar mechanism at all temperatures, with either dissociative adsorption of water or dissociative adsorption of methanol as the rate-determining step. In the case of glycerol oxidation on platinum, the mechanism changes at 110 °C. At low temperatures dissociative adsorption of water or dissociative adsorption of glycerol is suggested to be the rate-determining step. At higher temperatures, a significant decrease in onset potential was observed and the glycerol is suggested to selectively oxidize to glyceraldehyde or dihydroxyacetone, with dissociative glycerol adsorption as the rate-determining step.

1. Introduction

Use of direct alcohol fuel cells (DAFC) offers an attractive alternative to the full implementation of the hydrogen economy [1]. However, organic fuels suffer from sluggish kinetics, electrode poisoning, and fuel crossover through the membrane. Understanding the reaction mechanism at the operating temperature is essential to improvement of the kinetics, and measurement over a wide range of temperatures enables activation energies to be obtained. High temperature aqueous electrochemistry has been reviewed [2,3], and has been used for decades to study corrosion processes [4], reference electrodes [5–7], transport properties [8–10], nuclear materials [11], and to study methods for pH measurements [12,13]. The method presented in this work builds on previous experimental activities with pressurized autoclaves [14–16] for studies of alcohol oxidation. The method facilitates quick acquisition of kinetic information at several temperatures. We demonstrate that a self-pressurized autoclave can study alcohol oxidation at temperatures up to 140 °C under the high-purity conditions needed to get quality kinetic data at noble-metal electrodes.

The method here builds on previous methods using pressurized autoclaves to study alcohol oxidation [14–16], but also facilitates fast acquisition of kinetic properties at several temperatures. In this work, we demonstrate that a self-pressurized autoclave can study alcohol oxidations at temperatures up to 140 °C under the high-purity conditions needed to get quality kinetic data at noble-metal electrodes. This system has the advantage that aqueous electrochemistry can be run at temperatures above the normal boiling point of water.

Two alcohols with distinctly different volatilities and kinetics, methanol and glycerol, were chosen to demonstrate the method. These fuels have a high volumetric energy density, 4.3 and 6.3 kWh L^{-1}, compared to compressed hydrogen at 700 bar, which has a volumetric energy density of 1.3 kWh L^{-1}. Methanol is a single-carbon molecule that is widely studied as a potential DAFC fuel candidate. The reaction mechanism of methanol oxidation has been well studied, e.g. [17–20], and it is a simple molecule with the potential for high CO_2 yield. However, it is volatile and

* Corresponding author. Tel.: (+47) 73 59 40 42.
E-mail addresses: thomhol@uvic.ca (T. Holm), perkrid@statoil.no (P.K. Dahlstrøm), odne.s.burheim@hist.no (O.S. Burheim), svein.sunde@ntnu.no (S. Sunde), dharr@uvic.ca (D.A. Harrington), frode.seland@ntnu.no (F. Seland).

http://dx.doi.org/10.1016/j.electacta.2016.11.130
0013-4686/

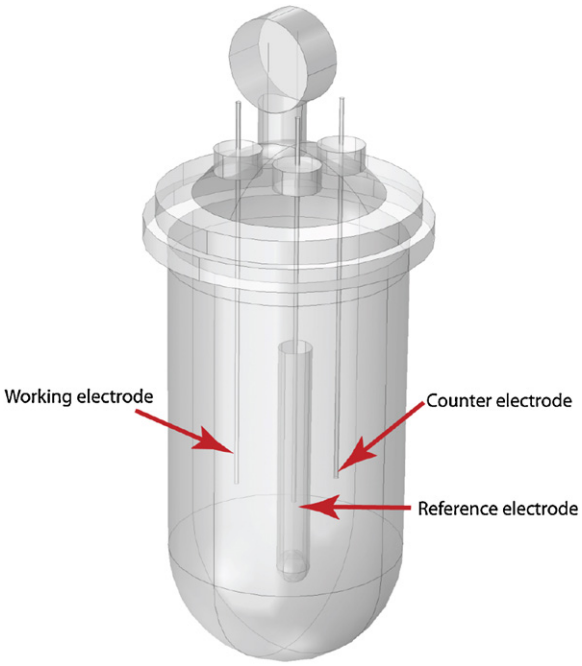

Fig. 1. Cell setup for the autoclave.

has high vapour pressures above its normal boiling point of 64.7 °C, which complicates high temperature operation with liquid reactants. Glycerol is a three-carbon alcohol molecule that has attracted increasing interest as a potential fuel candidate in the last decade. This interest has arisen due to glycerol being readily available at low cost, as it is a byproduct of biodiesel production [21]. Glycerol has the advantage of a low vapour pressure below its normal boiling point of 290 °C. Complete electrooxidation of glycerol to CO_2 demands carbon-carbon bond breaking, resulting in low yields of CO_2 at room temperature on polycrystalline Pt [22]. However, this is not necessarily a problem as the low cost of glycerol makes selective oxidation to partial oxidation products such as glyceraldehyde or dihydroxyacetone a profitable process [23].

In this work, we present kinetic data for oxidation of methanol and glycerol at Pt electrodes in sulfuric acid electrolyte for temperatures up to 140 °C. The kinetic parameters determined include onset potentials, E_{onset}, Tafel slopes, b_T, and activation energies, E_A, as determined from cyclic voltammetry. The information available from these studies of alcohol oxidation at elevated temperatures should be useful in optimizing fuel cell operation.

2. Experimental

The pressurized system consists of a 300 mL glass autoclave with a PTFE lid (Büchi AG), Fig. 1, and is described in more detail in reference [24]. This setup allowed for operation up to a temperature of 200 °C or a pressure of 10 bar. The electrical connection to the inside of the autoclave used a PTFE seal around a twist free piano wire (d-6 mm K&S Engineering) that could be fitted into the 1/4 inch Swagelok connection. The reference electrode (within the cell) was a reversible hydrogen electrode (RHE) consisting of a Pt mesh inside a glass tube sealed at the top. Hydrogen was produced at the Pt mesh in an electrolyte consisting of only supporting electrolyte, ensuring equilibrium between H^+ in solution and the hydrogen gas at the platinum electrode. Constant pressure at the reference electrode was obtained by slow heating rates ensuring an equal increase of pressure in all compartments. This keeps the hydrogen partial pressure constant at 1 bar (as when produced at room temperature). All potentials are referred to this reference electrode unless otherwise specified. The counter electrode was a Pt mesh spot-welded to a Pt wire sealed in glass. The working electrode was a Pt wire electrode sealed in glass. The area of the working electrode was 0.08 cm^2 in the fuel-free experiments, 0.05 cm^2 in the glycerol oxidation experiments, and 0.005 cm^2 in the methanol oxidation experiments as determined from the charge affiliated to the hydrogen underpotential deposition in alcohol-free electrolyte at room temperature before each experimental series. The much higher current densities for methanol oxidation made it necessary to use a smaller electrode to reduce the effect of solution resistance.

The glassware and electrodes were cleaned in hot sulfuric acid before each run and rinsed at least twice in high purity water (Millipore Milli-Q). The autoclave was filled with 200 mL of electrolyte containing the alcohol, sealed off, and put in a temperature-controlled oil bath. Due to the corrosive nature of the electrolyte and the limited number of inputs to the autoclave, the temperature was controlled and measured in the oil bath. Therefore, the relationship between the electrolyte temperature and the oil bath temperature was determined in a calibration run using 200 mL of high purity water.

The supporting electrolyte was 0.5 mol dm^{-3} sulfuric acid (Seastar Chemicals Baseline® 93 - 98%). The alcohol oxidation experiments used 1 mol dm^{-3} solutions of methanol (Acros electronic use grade 99.8%) or glycerol (Anachemia ACS grade 99.5%) in the supporting electrolyte. A Gamry Ref 600 potentiostat was used to control the potential between the working and reference electrode. The electrodes were cycled 100 times between 0.05 and 1.4 V at 200 mV s^{-1} prior to all experiments at elevated temperatures. A series of experiments at different temperatures was conducted in a single session while ramping the temperature in the oil bath at 10 K hr^{-1}. A series of cyclic voltammograms between 0.05 and 1.4 V run at sweep rates between 20 mV s^{-1} and 1000 mV s^{-1} started every 30 min and lasted less than 10 min. In addition, potentiostatic electrochemical impedance spectroscopy was used to estimate the solution resistance, which was found to be small at all temperatures and neglected in the analysis. In summary, a series of experiments acquired the data at 5 K intervals, with a temperature uncertainty of ±2 K. The current densities were calculated based on the estimated electrochemically-active surface area, assuming the charge of the hydrogen adsorption peaks between to be 220 $\mu C\,cm^{-2}$.

The metal-solution potential difference at the RHE changes with temperature, and so measurements of the apparent activation energy, $E_{A,app}$, at a fixed potential vs RHE are not determined only by the working electrode reaction. They were corrected to represent the activation energy for constant working-electrode metal-solution potential difference, E_A, according to the method of Protsenko and Danilov [25], Eq. (1).

$$E_A = E_{A,app} - \alpha F T \frac{dE_{RHE}}{dT} \quad (1)$$

For the correction term, α was assumed to be 0.5, T was the average temperature of the temperatures used for the regression, and dE_{RHE}/dT was estimated as $\Delta S^o_{SHE}/F = 0.87$ mV K^{-1} [26], where ΔS^o is for the reaction $H^+ + e^- \rightleftharpoons \frac{1}{2}H_2$. The small temperature dependence of the activity part of the Nernst equation at the RHE was neglected.

3. Results and discussion

3.1. Platinum surface processes at high temperatures

Fig. 2a-c compare the cyclic voltammograms of Pt in sulfuric acid electrolytes without alcohol (a), withss methanol (b), and with glycerol (c) at 80 °C. The platinum voltammogram shows the well-known regions for underpotential hydrogen adsorption/desorption (0.05 V - 0.3 V), double-layer charging (0.3 V - 0.8 V), and platinum

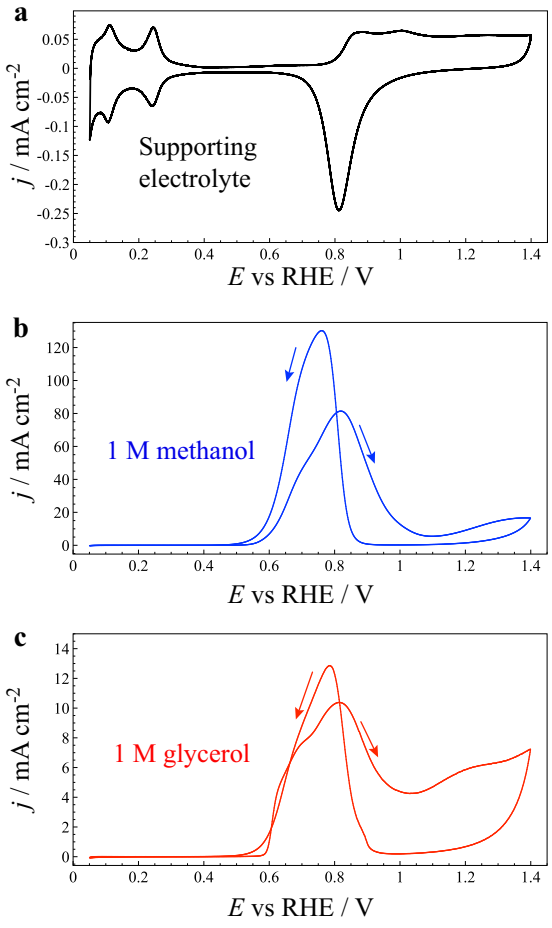

Fig. 2. Cyclic voltammogram for platinum in 0.5 mol dm^{-3} H_2SO_4 only (a), solution containing 1 mol dm^{-3} methanol (b - blue), and solution containing 1 mol dm^{-3} glycerol (c - red). Scan rate is 50 mV s^{-1} and temperature is 80 °C. Note the different scales for the current density.

oxide formation and reduction (0.8 V - 1.4 V) [27]. The addition of methanol or glycerol, Fig. 2a-b, gives a large increase in current and the alcohol oxidation processes dominate the total current response. However, the influence of the platinum oxide formation is seen as a large drop in current at potentials higher than 0.9 V, even though the overpotential for alcohol oxidation is steadily increasing. The current increases sharply again during the negative-going sweep direction as the platinum oxide is reduced and exposes active Pt sites for alcohol oxidation.

When the temperature is increased for platinum in sulfuric acid, it mainly influences the platinum oxide formation and reduction processes, Fig. 3. This was also observed previously over a lower temperature range [28], and to temperatures up to 200 °C for electrically heated electrodes [29]. Although the extent of Pt oxidation increases at higher temperatures, the onset potential change is small and between 0.81 and 0.85 V for all temperatures. Therefore, the platinum oxide should have little influence on the alcohol oxidation reaction at potentials relevant for fuel cells, i.e., below 0.7 V. However, the temperature may influence chemical processes such as anion adsorption and water adsorption without a visible influence on the voltammograms. These processes may influence the alcohol oxidation current.

3.2. Temperature dependence of methanol oxidation

In the presence of methanol, large anodic currents arise as seen in Fig. 2b. The complete oxidation of methanol to CO_2, Eq. (2), has

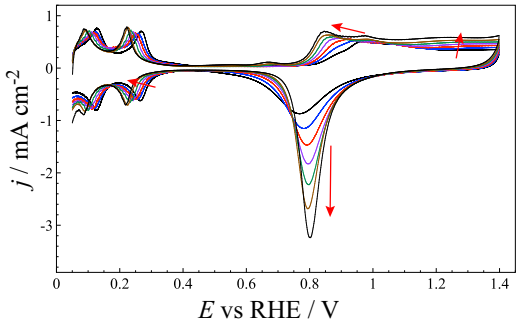

Fig. 3. Temperature dependence of Pt cyclic voltammograms in sulfuric acid. Scan rate is 500 mV s^{-1}. Temperatures are 25 °C (black small current), 40 °C (blue), 60 °C (red), 80 °C (purple), 100 °C (green), 120 °C (brown), and 140 °C (black large current). Red arrows indicate the trend as temperature is increased.

a standard potential of 0.016 V vs SHE. However, as seen in the voltammogram in Fig. 2b, the methanol oxidation reaction rate is insignificant until about 0.6 V.

$$CH_3OH + H_2O \rightarrow CO_2 + 6H^+ + 6e^- \quad (2)$$

The reaction mechanism of methanol oxidation has been reviewed [17–20]. A suggested pathway for producing CO_2 is given in Eqs. (3)–(6), and involves reactions such as dissociative adsorption of methanol (Eq. (3)) and water (Eq. (5)), oxidation of methanol to adsorbed CO (Eq. (3)–(4)), surface reaction between adsorbed molecules (Eq. (6)), diffusion of the reactants and products in the solution, and surface diffusion of the adsorbed species. A second "direct" pathway also occurs, which does not involve adsorbed CO as an intermediate [17,19,30]. In addition, at room temperature only about 40% of the total current goes towards CO_2 production [31,32], and products such as formaldehyde and formic acid are found [31,33–35]. Accordingly, the sequence of reactions presented is a simplified picture of the actual mechanism.

$$CH_3OH \leftrightarrows CH_2OH(ads) + H^+ + e^- \quad (3)$$

$$CH_2OH(ads) \leftrightarrows CO(ads) + 3H^+ + 3e^- \quad (4)$$

$$H_2O \leftrightarrows OH(ads) + H^+ + e^- \quad (5)$$

$$CO(ads) + OH(ads) \rightarrow CO_2 + H^+ + e^- \quad (6)$$

The large overpotentials suggests that the surface is either blocked by a strongly adsorbed species or is kinetically not favorable for one or more of the reactions in Eqs. (3)–(6). The overall reaction is not expected to be mass-transport controlled at these concentrations [36], although a clear impact of mass transport has been seen before [37] due to an alteration in product distribution and hence, the current yield. At potentials below 0.6 V, IR studies show that the surface is largely covered by CO [38]. However, steady-state experiments indicate that the maximum surface is only about 70% of a monolayer [39,40], which arises because dehydrogenation of methanol to adsorbed CO requires three adjacent Pt sites [41,42]. Therefore, the surface is not blocked by a compact CO layer indicating that sites are still available for dissociative water adsorption. The reaction of CO to CO_2 (Eq. (6)), or the dissociative adsorption of water onto the surface (Eq. (5)) has to be the rate-determining step. An observed drop in overpotential when platinum is alloyed with a metal more active towards water adsorption supports this assumption of bifunctional surface [43,44]. Density functional theory (DFT) calculations suggest that dissociative water adsorption to OH is favorable above about 0.6 V vs SHE at room temperature on Pt(111) [45–48].

Although the potential-dependent adsorption of water (Eq. (5)) is rate-determining at low potentials, its rate increases into the peak starting at 0.6 V until another step becomes rate determining

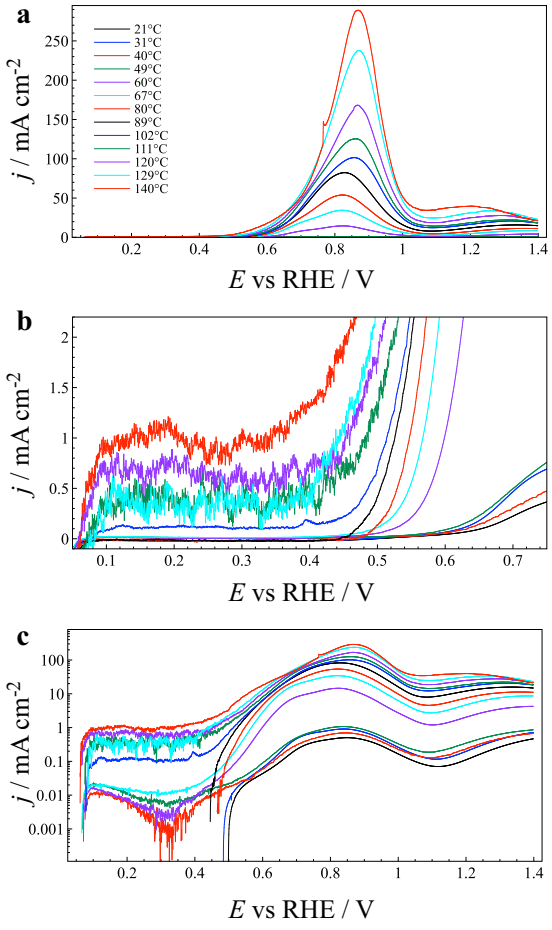

Fig. 4. Temperature dependence of methanol oxidation. Only the anodic scan direction of the voltammograms is shown. Scan rate 20 mV s^{-1}. (a) Full scale cyclic voltammograms, (b) expanded scale cyclic voltammogram highlighting the onset potentials, (c) logarithmic plots of current vs potential highlighting the Tafel slopes.

in line with previous mechanistic studies presented in the literature [49]. The surface coverage of CO at room temperature drops when the potential increases [50], indicating that the reaction is not dependent on adsorbed OH. IR studies at these potentials show the presence of large quantities of formate at the surface, HCHO(ads) [32]. This could indicate that an earlier step in the CO_2 formation mechanism or one of the mechanisms producing formaldehyde or formic acid is dominating. The rise in current density is halted at 0.85 V due to the Pt oxide formation, as discussed in Section 3.1. The decline in current density ceases at 1.0 V, where most of the surface is covered with platinum oxide [27]. The oxidized platinum surface results in low current densities until the oxide is reduced again. This oxide reduction starts at 0.9 V in the negative-going sweep, and initiates the large activity increase of methanol oxidation during the cathodic scan. The reaction then proceeds until the surface is largely covered with CO again, and water adsorption is again rate limiting.

An increase in temperature was found to increase the yield of CO_2 during methanol oxidation, greatly simplifying the reaction mechanism [31]. The voltammograms show a thousandfold increase in current density from 21 °C to 140 °C, Fig. 4a-c. Even though the increase in current density is large, the basic features in the voltammograms remain similar for all temperatures. There is a very low current until the onset of the oxidation, highlighted in Fig. 4b. An increase in temperature clearly influences the onset potentials, while the Tafel slopes are mostly constant at all temperatures. This indicates that a temperature increase does not have a large influence on the methanol oxidation mechanism on polycrystalline platinum in the temperature range studied. The onset potential, Tafel slopes, and activation energies derived from these data are discussed in more detail in Section 3.4.

3.3. Temperature dependence of glycerol oxidation

In the case of glycerol oxidation, in Fig. 2c, the voltammogram has many of the same features as for methanol oxidation in Fig. 2b, indicating that many of the same processes determine the measured current. There is little current until 0.6 V in the positive-going sweep, then a peak with a shoulder from 0.6 V to about 1 V, and then a drop in current to a plateau that persists until the reversal potential at 1.4 V. During the negative-going sweep, there is little current until 0.9 V, where a large oxidation peak is visible before the current drops to zero again at about 0.5 V. Complete oxidation of glycerol to CO_2 is a 14-electron process, shown in Eq. (7).

$$C_3H_5(OH)_3 + 3H_2O \rightarrow 3CO_2 + 14H^+ + 14e^- \quad (7)$$

However, a complete oxidation of glycerol to CO_2 is unlikely, and consequently, various partial oxidation products have been detected, including tartronic acid, gluconic acid, glyoxylic acid, formic acid, carbon monoxide, dihydroxyacetone, glyceraldehyde and glyceric acid [22,51,52]. The large variety of products is due to the difficulty of carbon-carbon bond cleavage, where factors like catalyst structure [53–55], reactant concentration and steric effects [56–59], support material [60–63], adatoms and alloyed catalysts [64–66], as well as pH [22,51,62,67,68] influence the mechanism. Low temperatures and overpotentials mainly produce glyceraldehyde, Eq. (8) (R = -CH(OH)CH_2OH), and glyceric acid, Eq. (9), with dihydroxyacetone as a minor product [22]. At higher overpotentials formic acid and carbon dioxide are found [22,52,69–73]. The tendency to favour oxidation to 2- and 4-electron transfer products at low temperatures and overpotentials is further supported by the fact that the flat electrodes used give low adsorption strength of the partly oxidized products and lower probability of readsorption due to the planar nature of the catalyst, as indicated by size studies on nanoparticles [58].

$$RCH_2(OH) \rightarrow RCHO + 2H^+ + 2e^- \quad (8)$$

$$RCH_2(OH) + H_2O \rightarrow RCOOH + 4H^+ + 4e^- \quad (9)$$

The equations above show that water as an oxygen donor is required to oxidize glycerol to glyceric acid but not to glyceraldehyde. The similarity with the methanol voltammetry in Fig. 2b suggests that dissociative water adsorption is important also for glycerol oxidation. The onset potential at lower temperatures is the same as for methanol, suggesting that water dissociation is again the rate-determining reaction, which would imply that production of glyceraldehyde is the dominating reaction at the onset potential and in the early stages of the main oxidation peak, as indicated by the work by Kwon et al. [22].

An increase in temperature has previously been shown to increase the yield of CO_2 [74]. Changing the temperature has a dramatic effect on the voltammograms as shown in Fig. 5a-c. The maximum current density is increased by a factor of 190 with a temperature change from 21 °C to 140 °C. In addition, the glycerol oxidation reaction is initiated at dramatically lower potentials at higher temperature. Furthermore, the glycerol oxidation has a clear shift of Tafel slope with increasing temperature from between 20 and 60 mV to between 160 and 200 mV. These observations indicate that glycerol oxidation mechanism changes as a function of temperature in the temperature range measured. The quantitative analysis of these changes in terms of the reaction mechanism are discussed in the next section.

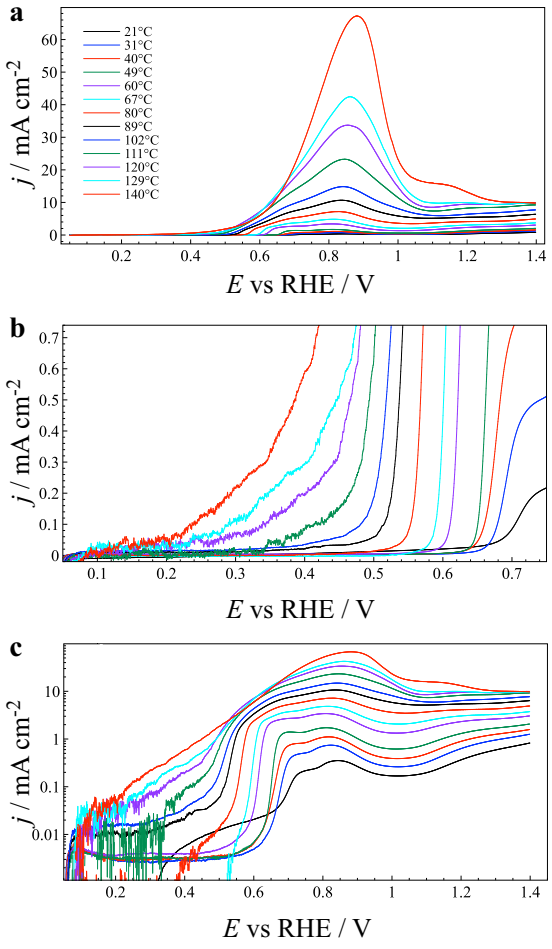

Fig. 5. Temperature dependence of glycerol oxidation. Only the anodic scan direction of the voltammograms is shown. Scan rate 20 mV s^{-1}. (a) Full scale cyclic voltammograms, (b) expanded scale cyclic voltammogram highlighting the onset potentials, (c) logarithmic plots of current vs potential highlighting the Tafel slopes.

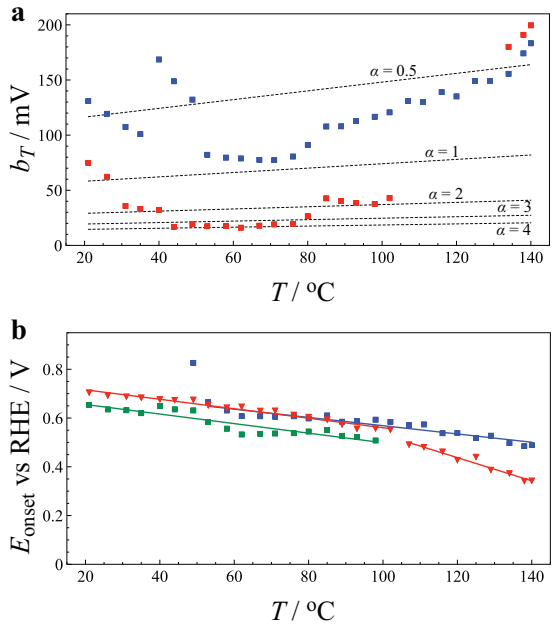

Fig. 6. Temperature dependence of Tafel slopes and onset potentials. Methanol oxidation (blue) and glycerol oxidation (red). (a) Experimental initial Tafel slopes are the filled squares. The dashed lines correspond to the theoretical Tafel slopes for the α values shown. (b) Onset potentials for glycerol at threshold current 0.1 mA cm^{-2} (red triangles), methanol at threshold current 0.1 mA cm^{-2} (green boxes), and methanol at threshold current 1 mA cm^{-2} (blue boxes). Full lines are the regression lines. The potentials are corrected for the temperature dependence of the reference electrode and are given relative to RHE at 298 K.

3.4. Kinetic analysis

Three parameters may be extracted from the temperature-dependent data and used to investigate the reaction mechanism. Onset potentials, E_{onset}, and Tafel slopes, b_T, were found directly from the slow-sweep voltammograms and are shown in Fig. 6. The activation energy was found at fixed potential from a series of voltammograms at different temperatures. In all cases only the initial stage of oxidation was analysed. The Tafel slopes were found from cyclic voltammograms at 20 mV s^{-1} as the slope of log(j) vs E, the slopes can be seen in Figs. 4c and 5c. The Tafel slope was defined as the initial slope after the onset potential. The onset potentials were defined as the potential at which the oxidation current exceeded a threshold value, given in the caption of Fig. 6.

Considering first the Tafel slopes for methanol oxidation, Tafel behaviour was found from the start of oxidation until about the peak potential. The Tafel slopes changed consistently with temperature and had values corresponding to transfer coefficients $\alpha = \ln(10)(RT/b_T F)$ ranging from 0.3 to 0.9. According to the conventional analysis, values close to 0.5 indicate that the first electron transfer step is rate determining, while values close to 1 indicate a rate-determining chemical step after the first electron transfer step. Assuming that the mechanism given in Eq. (3)–(6) dominates the current at all potentials and temperatures, the possible candidates are the dissociative methanol adsorption, Eq. (3), dissociative water adsorption, Eq. (5), or a surface diffusion step involving one of the adsorbed molecules in the reaction.

Looking at the Tafel slopes found for glycerol oxidation in Fig. 6a, there is a much larger change as the temperature is increased. The Tafel slopes for glycerol oxidation were not as constant as for methanol oxidation and for many temperatures they account for the sharp increase in current after the onset potential that can span less than 50 mV in some cases. Therefore, the low Tafel slope values in Fig. 6a resulting in high α values have high uncertainties. Starting at room temperature, the transfer coefficient, α, increases in value from 0.7 to 2 and then further to 3.5 - 4. Above 75 °C it firstly drops to about 2 and subsequently down to less than 0.5 at temperatures above 130 °C. Under the simplifying assumption that glyceraldehyde or glyceric acid are the main products at all temperatures [22], the α value may be used to narrow down the number of possible pathways. A low α value, such as at temperatures above 130 °C, indicates that the first dehydrogenation of glycerol may be rate determining. The high α values of 3.5 - 4 have numerous possibilities in terms of rate-determining steps, and are consistent with, but not limited to, glyceric acid dehydrogenation or the last electrochemical step in the production of glyceric acid as rate-determining step. For the intermediate α value of about 2, from 90 - 110 °C, a possible mechanism is two electrochemical steps followed by a chemical one, and a candidate rate-determining step is the desorption of glyceraldehyde. The α values found from the Tafel slopes are most valuable if the current is linear over several orders of magnitude, which is only fulfilled at 140 °C. Therefore, the low α values at these temperatures are a clear indication of a change in mechanism at higher temperatures.

Trend lines are added in Fig. 6b to visualize the relatively large shift in the onset potentials. The resulting slopes are between −1.7 and −2.0 mV K^{-1} for methanol oxidation at all temperatures and for glycerol oxidation at low temperatures. For glycerol, there is a sharp change in slope to −4.7 mV K^{-1} at temperatures above 110 °C,

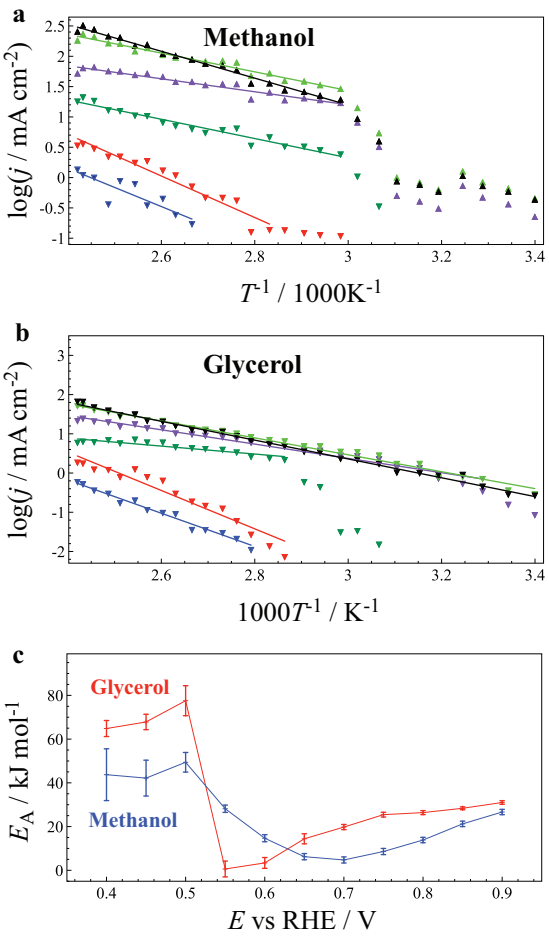

Fig. 7. Arrhenius plots and activation energies. (a), (b) Arrhenius plots for methanol and glycerol oxidation. Potentials vs RHE: 0.4 V (blue), 0.5 V (red), 0.6 V (green), 0.7 V (purple), 0.8 V (light green), 0.9 V (black). Lines are regression lines used to calculate the apparent activation energies. (c) Corrected activation energies for methanol (blue) and glycerol (red).

which leads to a much-reduced onset potential of about 0.35 V at 140 °C. The onset potentials taken together with the Tafel slopes create a consistent picture of the mechanisms. For methanol, consistent trends across the whole temperature range support a single dominant reaction mechanism at all temperatures. However, for glycerol, both Tafel slopes and onset potentials change at high temperatures indicating a change in mechanism. The decrease in the onset potential to the region where dissociative adsorption of water does not occur, as indicated by ab initio calculations [46–48] and measurements of the point of zero charge [45], suggests a switch to glyceraldehyde or dihydroxyacetone as a product. The α value of about 0.5 would be consistent with the first electron-transfer step rate limiting, and the second electron transfer in a fast step. A slow oxidative adsorption step followed by a fast oxidative desorption step to give glyceraldehyde is consistent with the Tafel slope, and would lead to low surface coverage, explaining the absence of the surface passivation that seems to dominate at lower temperatures.

The last kinetic parameter available from the cyclic voltammetry data is the activation energy. Apparent activation energies were extracted from the slopes of log(j) vs 1/T plots recorded at 20 mV s^{-1} for fixed potential vs RHE and are shown in Fig. 7a-b. This sweep rate represents a practical compromise between very slow steady state measurements and faster measurements that reduce the accuracy of the activation energies. Similar sweep rates have been used for mechanistic studies in the literature [20]. The apparent activation energies were converted to the activation energies at fixed working-electrode metal-solution potential difference and given in Fig. 7c. The values found ranged from 4.7 to 49 kJ mol^{-1} for methanol oxidation and from 0.6 to 78 kJ mol^{-1} for glycerol oxidation.

The lack of temperature dependence for values close to zero might suggest mass transport control. However, a quick calculation of the limiting current assuming a 2-electron transfer reaction and an irreversible reaction using cyclic voltammetry, the input values of a concentration of 1 mol L^{-1}, diffusion coefficient of 10^{-9} m^2 s^{-1} [75], a sweep rate of 20 mV s^{-1}, and a transfer coefficient of 0.5 gives a mass transport limited current of 270 mA cm^{-2} at room temperature ($j_p = 2.99\times10^{-5} n(\alpha n)^{1/2} c D^{1/2} \nu^{1/2}$). This maximum value is significantly higher than the peak currents for glycerol oxidation at all temperatures indicating that mass transport does not significantly influence the current for these reactions. However, the large amount of glycerol present in solution may stabilize different oxidation products on the surface, or hinder water adsorption. This would efficiently impede further oxidation and adsorption of glycerol giving a de facto mass transport limitation as indicated by the work of Gomes et al on concentration effects [56]. On the other hand, the true activation energies may be significantly influenced by the correction factor for the temperature dependence of the reference electrode, perhaps due to the assumption of a constant transfer coefficient.

At low overpotentials, only high temperature data was used for the Arrhenius plots because there is essentially no reaction at low temperatures. At low overpotentials, the activation energy is high for both methanol oxidation (40 - 50 kJ mol^{-1}) and for glycerol oxidation (60 - 80 kJ mol^{-1}). Relatively high activation energies (> 60 kJ mol^{-1}) suggest a bond breaking process [43,76,77]. This supports the previous findings from Tafel slopes and onset potentials that either dissociative water adsorption or dissociative alcohol adsorption is rate determining. At higher overpotentials, a sharp drop in activation energy is observed, indicating a change in the mechanism. Low activation energies for both methanol oxidation (5 - 30 kJ mol^{-1}) and glycerol oxidation (5 - 35 kJ mol^{-1}) suggest that an associative adsorption or surface diffusion step is rate determining [38,78–83]. Conclusions based on electrochemical activation energies are uncertain because they depend to some extent on the potential and on the charges of the species involved. However, combining the results in Fig. 7 with the findings from Tafel slopes and onset potentials increases confidence in the assignment of the rate-determining reaction steps.

In the case of methanol oxidation, the mechanism seems to be stable as a function of both temperature and potential, and this indicates that either dissociative water adsorption, Eq. (5), or dissociative methanol adsorption, Eq. (3), is the rate-determining step in all cases.

For glycerol oxidation, the picture is more complicated and the rate-determining step changes both as a function of temperature, Fig. 6, and as a function of potential, Fig. 5. At low temperatures, glycerol oxidation seems to be limited in the same way as methanol oxidation. At high temperatures, the same mechanism seems to span the whole potential range, and the kinetic parameters suggest that the main oxidation product is glyceraldehyde or dihydroxyacetone.

4. Conclusions

This work demonstrates a method for performing high purity aqueous electrochemistry at temperatures above the boiling point of water using commercially available equipment. This allows for the study of alcohol oxidation at high rates and at temperatures relevant for fuel cell operation. It uses efficient acquisition of data over a wide temperature range and allows the determination of kinetic

parameters such as onset potentials, Tafel slopes and activation energies.

Methanol oxidation was studied at temperatures up to 140 °C. The voltammograms and kinetic parameters show that the dissociative adsorption of water or the oxidation dissociative adsorption of methanol, is the rate-determining step at all temperatures and at potentials below the main peak.

Glycerol oxidation was studied over the same temperature range. For temperatures below 110 °C, the rate-determining step is the same as for methanol oxidation. However, the glycerol oxidation reaction mechanism changes above 110 °C, with the Tafel slope indicating that dissociative glycerol adsorption is the rate-determining step and the final reaction product is glyceraldehyde or dihydroxyacetone. This change in mechanism is associated with a large decrease in overpotential. This suggests that at the higher temperatures studied here, glycerol may be a viable fuel in a fuel cell, or in an electrochemical reactor to selectively oxidize glycerol to glyceraldehyde or dihydroxyacetone. Further studies will be required to chemically verify the high-temperature reaction product.

Acknowledgements

Financial support from the Natural Sciences and Engineering Research Council of Canada (discovery grant 37035), the Research Council of Norway (project 221899), the University of Victoria, and the Norwegian University of Science and Technology is gratefully acknowledged. This research was conducted in part under the Engineered Nickel Catalysts for Electrochemical Clean Energy project administered from Queen's University and supported by Grant No. RGPNM 477963-2015 under the Natural Sciences and Engineering Research Council of Canada (NSERC) Discovery Frontiers Program. Thomas Holm thanks the Faculty of Natural Sciences and Technology at Norwegian University of Science and Technology for the award of a scholarship.

Appendix A. Supplementary Data

Supplementary data associated with this article can be found, in the online version, at http://dx.doi.org/10.1016/j.electacta.2016.11.130.

References

[1] H. Liu, C. Song, L. Zhang, J. Zhang, H. Wang, D.P. Wilkinson, Journal of Power Sources 155 (2006) 95–110.
[2] D.D. Macdonald, Modern Aspects of Electrochemistry 11 (1975) 141–197.
[3] G. Wildgoose, D. Giovanelli, N. Lawrence, R. Compton, Electroanalysis 16 (2004) 421–433.
[4] R. Cowan, A. Kaznoff, Corrosion (Houston, TX, United States) 29 (1973) 123–132.
[5] B. Case, G. Bignold, Journal of Applied Electrochemistry 1 (1971) 141–146.
[6] D.D. Macdonald, Corrosion (Houston, TX, United States) 34 (1978) 75–84.
[7] D.D. Macdonald, A. Scott, P. Wentrcek, Journal of The Electrochemical Society 126 (1979) 908–911.
[8] W. Bogaerts, A. Van Haute, Journal of The Electrochemical Society 131 (1984) 68–72.
[9] A. McDonald, F.-R. Fan, A.J. Bard, Journal of Physical Chemistry 90 (1986) 196–202.
[10] L. Trevani, E. Calvo, H. Corti, Electrochemistry Communications 2 (2000) 312–316.
[11] Y. Chen, M. Urquidi-Macdonald, D.D. Macdonald, Journal of Nuclear Materials 348 (2006) 133–147.
[12] S. Hettiarachchi, P. Kedzierawski, D.D. Macdonald, Journal of The Electrochemical Society 132 (1985) 1866–1870.
[13] D. Midgley, Talanta 37 (1990) 767–781.
[14] A.J. Bard, W. Flarsheim, K. Johnston, Journal of The Electrochemical Society 135 (1988) 1939–1944.
[15] H. Nonaka, Y. Matsumura, Journal of Electroanalytical Chemistry 520 (2002) 101–110.
[16] A.P.M. Camargo, B.A.F. Previdello, H. Varela, E.R. Gonzales, Quimica Nova 33 (2010) 2143–2147.
[17] R. Parsons, T. VanderNoot, Journal of Electroanalytical Chemistry and Interfacial Electrochemistry 257 (1988) 9–45.
[18] S. Wasmus, A. Küver, Journal of Electroanalytical Chemistry 461 (1999) 14–31.
[19] T. Iwasita, Electrochimica Acta 47 (2002) 3663–3674.
[20] J.L. Cohen, D.J. Volpe, H.D. Abruna, Phys. Chem. Chem. Phys. 9 (2007) 49–77.
[21] C. Quispe, C. Coronado, J.A. Carvalho Jr., Renewable and Sustainable Energy Reviews 27 (2013) 475–493.
[22] Y. Kwon, K.J.P. Schouten, M.T.M. Koper, ChemCatChem 3 (2011) 1176–1185.
[23] S. Bagheri, N.M. Julkapli, W.A. Yehye, Renewable and Sustainable Energy Reviews 41 (2015) 113–127.
[24] T. Holm, P.K. Dahlstrøm, S. Sunde, D.A. Harrington, F. Seland, ECS Transactions 75 (2016) 1055–1061.
[25] V. Protsenko, F. Danilov, Journal of Electroanalytical Chemistry 651 (2011) 105–110.
[26] B.E. Conway, D.P. Wilkinson, Electrochimica Acta 38 (1993) 997–1013.
[27] B.E. Conway, Progress in Surface Science 49 (1995) 331–452.
[28] M. Alsabet, M. Grden, G. Jerkiewicz, Journal of Electroanalytical Chemistry 589 (2006) 120–127.
[29] A.S. Baranski, Analytical Chemistry 74 (2002) 1294–1301.
[30] E. Herrero, W. Chrzanowski, A. Wieckowski, The Journal of Physical Chemistry 99 (1995) 10423–10424.
[31] M. Chojak-Halseid, Z. Jusys, R.J. Behm, The Journal of Physical Chemistry C 114 (2010) 22573–22581.
[32] S. Liu, L. Liao, Q. Tao, Y. Chen, S. Ye, Phys. Chem. Chem. Phys. 13 (2011) 9725–9735.
[33] H. Wang, T. Löffler, H. Baltruschat, Journal of Applied Electrochemistry 31 (2001) 759–765.
[34] T.H.M. Housmans, A.H. Wonders, M.T.M. Koper, The Journal of Physical Chemistry B 110 (2006) 10021–10031.
[35] S. Celik, M.D. Mat, International Journal of Hydrogen Energy 35 (2010) 2151–2159.
[36] F. Seland, R. Tunold, D.A. Harrington, Electrochimica Acta 51 (2006) 3827–3840.
[37] F. Seland, R. Tunold, D.A. Harrington, Electrochimica Acta 55 (2010) 3384–3391.
[38] D. Kardash, J. Huang, C. Korzeniewski, Langmuir 16 (2000) 2019–2023.
[39] B. Beden, F. Hahn, S. Juanto, C. Lamy, J.-M. Leger, Journal of Electroanalytical Chemistry and Interfacial Electrochemistry 225 (1987) 215–225.
[40] F. Seland, D.A. Harrington, R. Tunold, Electrochimica Acta 52 (2006) 773–779.
[41] H.A. Gasteiger, N. Markovic, P.N. Ross, E.J. Cairns, The Journal of Physical Chemistry 97 (1993) 12020–12029.
[42] A. Cuesta, Journal of the American Chemical Society 128 (2006) 13332–13333.
[43] H.A. Gasteiger, N. Marković, P.N. Ross, E.J. Cairns, Journal of The Electrochemical Society 141 (1994) 1795–1803.
[44] N. Wakabayashi, H. Uchida, M. Watanabe, Electrochemical and Solid-State Letters 5 (2002) E62–E65.
[45] T. Iwasita, Z. Xia, Journal of Electroanalytical Chemistry 411 (1996) 95–102.
[46] A.B. Anderson, T. Albu, Journal of The Electrochemical Society 147 (2000) 4229–4238.
[47] J. Rossmeisl, J. Nørskov, C. Taylor, M. Janik, M. Neurock, Journal of Physical Chemistry B 110 (2006) 21833–21839.
[48] V. Viswanathan, H. Hansen, J. Rossmeisl, T. Jaramillo, H. Pitsch, J. Nørskov, The Journal of Physical Chemistry C 116 (2012) 4698–4704.
[49] Z. Jusys, R.J. Behm, Fuel Cell Catalysis, Electrocatalysis and Electrochemistry, John Wiley & Sons, Hoboken, New Jersey, pp. 421-425.
[50] Y. Chen, A. Miki, S. Ye, H. Sakai, M. Osawa, Journal of the American Chemical Society 125 (2003) 3680–3681.
[51] J.F. Gomes, G. Tremiliosi-Filho, Electrocatalysis 2 (2011) 96–105.
[52] P. Fernández, C. Martins, M. Martins, G. Camara, Electrochimica Acta 112 (2013) 686–691.
[53] J.F. Gomes, F.B.C. de Paula, L.H.S. Gasparotto, G. Tremiliosi-Filho, Electrochimica Acta 76 (2012) 88–93.
[54] Y. Zuo, L. Wu, K. Cai, T. Li, W. Yin, D. Li, N. Li, J. Liu, H. Han, ACS Applied Materials & Interfaces 7 (2015) 17725–17730.
[55] A.C. Garcia, M.J. Kolb, C. van Nierop y Sanchez, J. Vos, Y.Y. Birdja, Y. Kwon, G. Tremiliosi-Filho, M.T.M. Koper, ACS Catalysis 6 (2016) 4491–4500.
[56] J.F. Gomes, C. Martins, M. Janete Giz, G. Tremiliosi-Filho, G. Camara, Journal of Catalysis 301 (2013) 154–161.
[57] C.A. Angelucci, H. Varela, G. Tremiliosi-Filho, J.F. Gomes, Electrochemistry Communications 33 (2013) 10–13.
[58] J. Lei, X. Duan, G. Qian, X. Zhou, D. Chen, Ind. Eng. Chem. Res. 53 (2014) 16309–16315.
[59] J. González-Cobos, S. Baranton, C. Coutanceau, Journal of Physical Chemistry C 120 (2016) 7155–7164.
[60] J.F. Gomes, L.H.S. Gasparotto, G. Tremiliosi-Filho, Physical Chemistry Chemical Physics 15 (2013) 10339–10349.
[61] Y. Li, F. Zaera, Journal of Catalysis 326 (2015) 116–126.
[62] C. Xu, Y. Du, C. Li, J. Yang, G. Yang, Applied Catalysis B: Environmental 164 (2015) 334–343.
[63] L.S. Ribeiro, E.G. Rodriguez, J.J. Delgado, X. Chen, M.F.R. Pereira, J.J.M. Orfao, Ind. Eng. Chem. Res 55 (2016) 8548–8556.
[64] S. Hirasawa, Y. Nakagawa, K. Tomishige, Catalysis Science & Technology 2 (2012) 1150–1152.
[65] Y. Kwon, Y. Birdja, I. Spanos, P. Rodriguez, M.T.M. Koper, ACS Catalysis 2 (2012) 759–764.
[66] B. Hasa, E. Kalamaras, E.I. Papaioannou, J. Vakros, L. Sygellou, A. Katsaounis, Electrochimica Acta 179 (2015) 578–587.

[67] L. Roquet, E.M. Belgsir, J.-M. Leger, C. Lamy, Electrochimica Acta 39 (1994) 2387–2394.
[68] J.-H. Zhang, Y.-J. Liang, N. Li, Z.-Y. Li, C.-W. Zu, Electrochimica Acta 59 (2012) 156–159.
[69] L.-W.H. Leung, M.J. Weaver, Langmuir 6 (1990) 323–333.
[70] J. Schnaidt, M. Heinen, D. Denot, Z. Jusys, R. Behm, Journal of Electroanalytical Chemistry 661 (2011) 250–264.
[71] C. Martins, M. Janete Giz, G. Camara, Electrochimica Acta 56 (2011) 4549–4553.
[72] P. Fernández, M. Martins, G. Camara, Electrochimica Acta 66 (2012) 180–187.
[73] C. Martins, P. Fernández, H. Troiani, M. Martins, G. Camara, Journal of Electroanalytical Chemistry 717-718 (2015) 231–236.
[74] K. Ishiyama, F. Kosaka, I. Shimada, Y. Oshima, J. Otomo, Journal of Power Sources 225 (2013) 141–149.
[75] W. Hayduk, H. Laudie, AlChE Journal 20 (1974) 611–615.
[76] W. Chrzanowski, A. Wieckowski, Langmuir 14 (1998) 1967–1970.
[77] T.H. Madden, E.M. Stuve, Journal of The Electrochemical Society 150 (2003) E571–E577.
[78] M.W. Breiter, Journal of Electroanalytical Chemistry and Interfacial Electrochemistry 19 (1968) 131–136.
[79] D. Chu, S. Gilman, Journal of The Electrochemical Society 143 (1996) 1685–1690.
[80] J.B. Day, P.-A. Vuissoz, E. Oldfield, A. Wieckowski, J.-P. Ansermet, Journal of the American Chemical Society 118 (1996) 13046–13050.
[81] N.M. Marković, B.N. Grgur, P.N. Ross, The Journal of Physical Chemistry B 101 (1997) 5405–5413.
[82] A.B. Anderson, N. Neshev, R. Sidik, P. Shiller, Electrochimica Acta 47 (2002) 2999–3008.
[83] T. Kobayashi, P. Babu, J. Chung, E. Oldfield, A. Wieckowski, Journal of Physical Chemistry C 111 (2007) 7078–7083.